the oil–water interface and the MC plate. However, the adsorption layer of SDS molecules on the oil–water interface becomes thinner for lower surfactant concentrations at high flow velocities due to the diffusional transfer limitation, and the dispersed phase wets the MC plate. This leads to larger droplet formation and longer detachment times. The significant limitations of the diffusional transfer caused the MC wetting with the dispersed phase to become conspicuous at higher flow velocities for lower SDS concentrations.

The effect of interfacial viscoelasticity and the interfacial tension gradient cannot be neglected in these flow velocity ranges (2 mm/s for 0.05% SDS concentration, 2.6 mm/s for 0.1% SDS concentration). We use the term "interfacial viscoelasticity" here for the force resisting interface movement. Interfacial viscoelasticity can increase the effective viscosity of the droplet phase by more than an order of magnitude during conventional emulsification under specific conditions [6]. The time scale of the detachment process is close to τ_d, 10^{-3} s, at high flow velocities, although accurate determination of τ_d is difficult because it is affected by the surfactant concentration, and the actual surfactant concentration at the exit of MC depends on the diffusional transfer in the well. Therefore, we cannot deny the effect of the interfacial viscoelasticity on the droplet formation process. The interfacial viscoelasticity may resist the interface movement during the detachment process and could induce outflow of the dispersed phase. The interfacial tension gradient may also resist rupture of the interface during the detachment process through the Marangoni effect, as reported in a previous study [31]. The effects of interfacial viscoelasticity and the interfacial tension gradient may be of interest; however, we did not note any effects in this study.

4. Summary

We performed MC emulsification with various surfactant concentrations at different flow velocities of the dispersed phase to investigate the effect of interfacial tension on the dynamic behavior of emulsification. The experimental results indicated that interfacial tension does not affect the droplet diameter, but affects only the time-scale parameters for droplet formation. The droplet formation behavior at a 1% SDS concentration correlated with our previous study, but the droplet formation behavior at lower SDS concentrations (less than 0.3%) differed from that for a 1% SDS concentration. These results were interpreted from the standpoint of dynamic interfacial tension. Analyses of the diffusional transfer rate of the surfactant molecules and the time-scale of interface extension indicated that diffusional transfer in the well is the rate-determining step and that the concentration of surfactant at the exit of the MC is less than the initial concentration. The dynamic interfacial tension exceeded the equilibrium value under these conditions. This led to short detachment times and droplet formation caused by spontaneous transformation, even at high flow velocities of the dispersed phase. The effect of dynamic interfacial tension was significant, particularly at lower surfactant concentrations and higher flow velocities of the dispersed phase. The droplet formation behavior was also affected by wetting of the MC with the dispersed phase at lower SDS concentrations, inducing formation of larger droplets at high flow velocities. A time-scale analysis indicated that the effect of interfacial viscoelasticity cannot be disregarded. Our results for the effects of dynamic interfacial behavior are useful for designing an MC emulsification process and interpreting the MC emulsification phenomena.

Acknowledgments

This work was supported by the Nanotechnology Project, Ministry of Agriculture, Forestry and Fisheries, and the Program for Promotion of Fundamental Studies in Health Sciences of the Organization for Pharmaceutical Safety and Research of Japan.

References

[1] D.J. McClements, Food Emulsions: Principles, Practice, and Techniques, CRC, Boca Raton, 1999.
[2] E. Dickinson, An Introduction to Food Colloids, Oxford Univ. Press, Oxford, 1992.
[3] T.G. Mason, A.H. Krall, H. Gang, J. Bibette, D.A. Weitz, in: P. Becher (Ed.), Encyclopedia of Emulsion Technology, Vol. 4, Dekker, New York, 1996, p. 299.
[4] P. Walstra, in: P. Becher (Ed.), Encyclopedia of Emulsion Technology, Vol. 1, Dekker, New York, 1983, p. 57.
[5] W.J. Phillips, R.W. Graves, R.W. Flumerfelt, J. Colloid Interface Sci. 76 (1980) 350.
[6] E.H. Lucassen-Reynders, K.A. Kuijpers, Colloids Surf. 65 (1992) 175.
[7] T. Nakashima, M. Shimizu, M. Kukizaki, Key Eng. Mater. 61/62 (1991) 513.
[8] S.M. Joscelyne, G. Trägårdh, J. Membr. Sci. 169 (2000) 107.
[9] A.J. Abrahamse, A. van der Padt, R.M. Boom, W.B.C. de Heij, AIChE J. 47 (2001) 1285.
[10] V. Schröder, O. Behrend, H. Schubert, J. Colloid Interface Sci. 202 (1998) 334.
[11] V. Schröder, H. Schubert, Colloids Surf. A 152 (1999) 103.
[12] T. Kawakatsu, Y. Kikuchi, M. Nakajima, J. Am. Oil Chem. Soc. 74 (1997) 317.
[13] T. Kawakatsu, G. Trägårdh, Y. Kikuchi, M. Nakajima, H. Komori, T. Yonemoto, J. Surfact. Deterg. 3 (2000) 295.
[14] S. Sugiura, M. Nakajima, M. Seki, Langmuir 18 (2002) 3854.
[15] T. Kawakatsu, G. Trägårdh, C. Trägårdh, M. Nakajima, N. Oda, T. Yonemoto, Colloids Surf. A 179 (2001) 29.
[16] S. Sugiura, M. Nakajima, H. Ushijima, K. Yamamoto, M. Seki, J. Chem. Eng. Jpn. 34 (2001) 757.
[17] S. Sugiura, M. Nakajima, J. Tong, H. Nabetani, M. Seki, J. Colloid Interface Sci. 227 (2000) 95.
[18] S. Sugiura, M. Nakajima, H. Itou, M. Seki, Macromol. Rapid Commun. 22 (2001) 773.
[19] J. Tong, M. Nakajima, H. Nabetani, Y. Kikuchi, J. Surfact. Deterg. 3 (2000) 285.
[20] S. Sugiura, M. Nakajima, S. Iwamoto, M. Seki, Langmuir 17 (2001) 5562.
[21] S. Sugiura, M. Nakajima, M. Seki, Langmuir 18 (2002) 5708.

[22] S. Sugiura, M. Nakajima, N. Kumazawa, S. Iwamoto, M. Seki, J. Phys. Chem. B 106 (2002) 9405.
[23] Y. Kikuchi, K. Sato, H. Ohki, T. Kaneko, Microvascular Res. 44 (1992) 226.
[24] M. Sasaki, T. Yasunaga, N. Tatsumoto, Bull. Chem. Soc. Jpn. 50 (1977) 858.
[25] A. Bonfillon, D. Langevin, J. Colloid Interface Sci. 168 (1994) 497.
[26] B. Lindman, M.-C. Puyal, N. Kamenka, R. Rymdén, P. Stilbs, J. Phys. Chem. 88 (1984) 5048.
[27] P.M. Vlahovska, K.D. Danov, A. Mehreteab, G. Broze, J. Colloid Interface Sci. 192 (1997) 194.
[28] V.B. Fainerman, E.H. Lucassen-Reynders, Adv. Colloid Interface Sci. 96 (2002) 295.
[29] T. Kawakatsu, H. Komori, M. Nakajima, Y. Kikuchi, T. Yonemoto, J. Chem. Eng. Jpn. 32 (1999) 241.
[30] I. Kobayashi, M. Nakajima, K. Chun, Y. Kikuchi, H. Fujita, AIChE J. 48 (2002) 1639.
[31] P. Walstra, Chem. Eng. Sci. 48 (1993) 333.

Available online at www.sciencedirect.com
SCIENCE DIRECT®
Journal of Colloid and Interface Science 270 (2004) 221–228
JOURNAL OF Colloid and Interface Science
www.elsevier.com/locate/jcis

Preparation characteristics of water-in-oil-in-water multiple emulsions using microchannel emulsification

Shinji Sugiura,[a,b,c] Mitsutoshi Nakajima,[a,*] Koji Yamamoto,[a] Satoshi Iwamoto,[a] Tatsuya Oda,[d] Mitsuo Satake,[e] and Minoru Seki[f]

[a] *National Food Research Institute, Kannondai 2-1-12, Tsukuba, Ibaraki 305-8642, Japan*
[b] *The Organization for Pharmaceutical Safety and Research, Chiyoda Ku, Tokyo 100-0013, Japan*
[c] *Radiology Division, National Cancer Center Hospital East, Kashiwa, Chiba 277-8577, Japan*
[d] *Department of Surgery, Institute of Clinical Medicine, University of Tsukuba, Tsukuba, Ibaraki 305-8573, Japan*
[e] *Diagnostics Radiology Division, National Cancer Center Hospital, Chuo Ku, Tokyo 104-0045, Japan*
[f] *Department of Chemistry and Biotechnology, The University of Tokyo, Bunkyo-ku, Tokyo 113-8656, Japan*

Received 18 March 2003; accepted 1 August 2003

Abstract

Microchannel (MC) emulsification is a novel technique for preparing monodispersed emulsions. This study demonstrates preparing water-in-oil-in-water (W/O/W) emulsions using MC emulsification. The W/O/W emulsions were prepared by a two-step emulsification process employing MC emulsification as the second step. We investigated the behavior of internal water droplets penetrating the MCs. Using decane, ethyl oleate, and medium-chain triglyceride (MCT) as oil phases, we observed successful MC emulsification and prepared monodispersed oil droplets that contained small water droplets. MC emulsification was possible using triolein as the oil phase, but polydispersed oil droplets were formed from some of the channels. No leakage of the internal water phase was observed during the MC emulsification process. The internal water droplets penetrated the MC without disruption, even though the internal water droplets were larger than the resulting W/O/W emulsion droplets. The W/O/W emulsion entrapment yield was measured fluorometrically and found to be 91%. The mild action of droplet formation based on spontaneous transformation led to a high entrapment yield during MC emulsification.

Keywords: Microchannel emulsification; Monodispersed emulsion; Droplet formation; Multiple emulsion; Water-in-oil-in-water emulsion; Double emulsion; Entrapment yield; Viscosity

1. Introduction

Multiple emulsions have been studied since 1925, when Seifriz pioneered this work [1]. A water-in-oil-in-water (W/O/W) emulsion consists of internal water droplets dispersed within larger oil droplets, which themselves have been dispersed in an external aqueous continuous phase. As Sherman noted [2], a multiple emulsion is obtained unexpectedly during ordinary emulsification procedures at high concentrations of the dispersed phase or the emulsifying agent, due to either phase inversion [1,3], or to the migration of the emulsifying agent between the two phases of the emulsion [4]. The two-step emulsification method is a reliable method for preparing W/O/W emulsions [5]. The first step in emulsification, providing the ordinary W/O emulsion, was accomplished with a hydrophobic surfactant (low HLB). The second step, providing the W/O/W dispersion, was then carried out by mixing the W/O emulsion within an aqueous solution of hydrophilic surfactant (high HLB).

W/O/W emulsions have primarily been investigated as vehicles for various hydrophilic drugs (vitamins, hormones, and enzymes) that are expected to have prolonged release profiles [6,7]. Multiple emulsions designed as drug delivery systems would be significant in the controlled release of oral, topical, or parenteral administrations when the stability and release mechanisms can be more clearly understood and monitored.

Recently, research has been conducted to create stable multiple emulsions [8–11]. Stability of W/O/W emulsions is generally understood as the resistance of the individual globules to coalescence. The breakdown of a W/O/W emulsion

* Corresponding author.
E-mail address: mnaka@nfri.affrc.go.jp (M. Nakajima).

0021-9797/$ – see front matter
doi:10.1016/j.jcis.2003.08.021

is described through several possible mechanisms [12], including (i) coalescence of the internal aqueous droplets into larger internal droplets; (ii) coalescence of the oil droplets suspended in the external aqueous phase; (iii) expulsion of the internal droplets following rupture of the thin oil films during the interaction of the internal and external aqueous phases; and (iv) swelling or shrinking due to water permeation through the oil membrane by diffusion.

Monodispersed multiple emulsions are useful for both industrial applications and basic studies. Rheology, appearance, chemical reactivity, and physical properties are influenced by both the average size and size distribution, and drug-release properties from multiple emulsions depend on their size. Furthermore, monodispersed emulsions can be very effective in determining the resistance to coalescence of an emulsion due to the ease of observation, and in detecting the water permeation through the oil membrane by diffusion. If the droplet diameter distribution is narrow, the effect of Ostwald ripening is reduced because the effective Laplace pressure is low.

Monodispersed emulsions can be obtained by fractionation from polydispersed emulsion, but repeated operations are required [13,14]. Several research groups are investigating how to produce quasi-monodisperse W/O/W emulsions. Membrane emulsification, in which the pressurized dispersed phase permeates a microporous membrane and forms emulsion droplets, enables us to produce monodispersed emulsions with a coefficient of variation of approximately 10% [15]. This technique has been applied to W/O/W emulsions [16–18]. However, it is not clear how internal water droplets penetrate through the membrane pore. Mason and Bibette proposed that the shear rupturing in couette flow is applicable to producing monodisperse emulsions [19]. This technique has been applied to preparing quasi-monodispersed W/O/W emulsions [20].

Recently, we proposed a novel method for making monodisperse emulsion droplets using a microfabricated channel array [21]. This emulsification technique is called microchannel (MC) emulsification. Oil-in-water emulsions with a coefficient of variation of less than 5% and a droplet size of 3 to 100 μm have been successfully prepared using this technique. The droplet size is controlled by MC geometry [22,23]. An advantage of this technique is direct observation of emulsification through a microscope [21]. We have applied this technique to preparing several types of oil-in-water emulsions, water-in-oil emulsions [25,26], lipid microparticles [27], and polymer microparticles [28]. A disadvantage is its low production rate. Usually, less than 1 ml/h of dispersed phase can be emulsified. A straight-through type MC has been devised to scale this technique up, and the droplet formation volume rate reached 6.5 ml/h of dispersed phase per MC plate [24]. Further scaling up is under way.

MC emulsification exploits the interfacial tension, the dominating force on a micrometer scale, as the driving force for droplet formation [29]. During the droplet formation, the distorted dispersed phase is spontaneously transformed into spherical droplets by interfacial tension. The dispersed phase is forced into a distorted (elongated) disk-like shape in the MC. This distorted disk-like shape is the essential point for spontaneous transformation since the disk-like shape has a higher interface area than a spherical shape, resulting in instability from the viewpoint of interface free energy. The dispersed phase with disk-like shape spontaneously transforms into spherical droplets. Therefore, the droplets are formed without shear by continuous phase flow, and the required energy input is very low compared with conventional emulsification techniques. The mechanism is similar to the breakup of cylindrical flow at the point where transformation is caused by interfacial tension [30]. Our previous study showed that the droplet diameter can be predicted from the MC structure based on the droplet formation mechanism [23]. The MC structure also affects the emulsion productivity [31]. The droplet formation behavior drastically changes above the critical flow velocity, and the critical flow velocity can be predicted by the critical capillary number [32]. The droplet formation is determined by the balance between the interfacial tension and viscous force.

In this study, W/O/W emulsions are prepared by a two-step emulsification employing MC emulsification as the second step. The mild action of MC emulsification, in which droplets are formed without shear by continuous phase flow, is expected to lead to a high entrapment yield of multiple emulsions. Although MC emulsification is the preferred first step, we used a homogenizer for the first step emulsification because of the limited production rate of MC emulsification. We prepared W/O/W emulsions with monodispersed oil droplets using MC emulsification by pressurizing the premixed W/O emulsions into the external water phase through the MC. A premixed polydispersed emulsion enables analyzing the behavior of the contained water droplets penetrating the MC in the second emulsification step. We then fluorometrically investigated the entrapment yield of the resulting W/O/W emulsion.

2. Materials and methods

2.1. Materials

Decane and ethyl oleate were purchased from Wako Pure Chemical Ind. (Osaka, Japan). Medium-chain triglyceride (MCT), with a fatty acid carbon number ranging from 8 to 10, was supplied by Taiyo Kagaku Co. Ltd. (Mie, Japan). Triolein (purity > 90%) was supplied by Nippon Lever B.V. (Tokyo, Japan). These were used as oil phases. Tris–HCl buffered (0.2 M, pH 9) Milli-Q water was used as internal and external water phases. Salt added in the internal water phase prevents the rapid coarsening of the W/O emulsion; salt added in the external phase balances the osmotic pressure. Tetraglycerin-condensed ricinoleic acid ester (CR-310, HLB < 1) is a suitable surfactant for preparing W/O emul-

sions. It was supplied by Sakamoto Yakuhin Kogyo Co. Ltd. (Osaka, Japan), and used to stabilize the premixed W/O emulsions. Pentaglycerin monolaurate (PGML; Sun soft A-121E; HLB = 12) was supplied by Taiyo Kagaku Co. Ltd., and was used to stabilize the O/W emulsion. Fluorescent dye (calcein) was purchased from Sigma Chemical Co. (St. Louis, MO, USA). Cobalt chloride ($CoCl_2$) was purchased from Kanto Chemical Co. Inc. (Tokyo, Japan). Calcein and $CoCl_2$ were used to determine the entrapment yields.

2.2. First-step emulsification

The first-step emulsification consists of preparing premixed polydisperse W/O emulsions. The premixed W/O emulsions were prepared using a homogenizer (Polytron PT-MR 3000; Kinematica AG, Littau, Switzerland). The homogenizer rotation speed and mixing time were controlled, as the premixed W/O emulsions have droplets with diameters from several to 100 μm. This wide range of droplet diameter distribution is useful for observing the variously sized internal water droplets penetrating through MCs.

2.3. MC emulsification

MC emulsification was used for the second step. The laboratory-scale apparatus for MC emulsification consists of a silicon MC plate, an MC module, and liquid chambers supplying continuous and dispersed phases [21]. Figure 1 depicts the experiment setup and schematic flow of the premixed W/O emulsion phase through the silicon MC. The emulsification was observed through the glass plate using a microscope with a differential interference contrast (DIC) mode and a fluorescent mode (DM IRM; Leica Microsystems AG, Wetzlar, Germany). In this study, a high-speed camera (Rabitt mini 2; Photoron, Tokyo, Japan), which can capture 600 frames/s, was also used to observe the emulsification. Figure 2 shows the silicon MC plate fabricated using photolithography and orientation-dependent etching processes [33]. The silicon MC plate measured 15 × 15 mm, and a 1-mm-diameter hole was produced at the center of the MC plate. Four 150-μm-high, 10-mm-long terrace lines were fabricated on the MC plate. In this study, 90 channels on each terrace line, 360 channels total, were fabricated and used. The MC module was initially filled with the external water phase. The W/O emulsion, which was pressurized by the head difference of the liquid chamber, entered the space between the silicon MC plate and the glass plate, and W/O/W droplets were formed from the MC. The prepared emulsion was recovered by an external water phase flow.

2.4. Measurement and analytical method

We determined the average diameters (D_a) (μm) and coefficients of variation (CV) (%) of the prepared emulsions from pictures of 100 droplets taken with the microscope

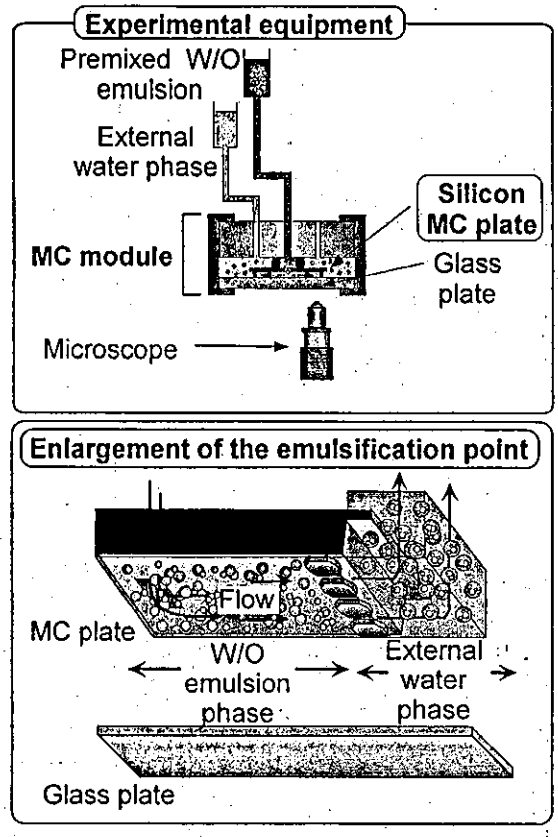

Fig. 1. Experimental setup and schematic flow of premixed W/O emulsion phase through the MC.

video system described above. The coefficient of variation is defined as

$$\mathrm{CV} = (\sigma/D_a) \times 100, \tag{1}$$

where σ is the standard deviation of the diameter (μm). Winroof (Mitani Corporation, Fukui, Japan) software was used to analyze the captured pictures. The viscosities of the organic solvents were measured with a Microviscometer (HAAKE, Karlsruhe, Germany). The viscosities of the oil phases containing 5% of the surfactant were measured.

Entrapment yield was determined fluorometrically by modifying the method used for determining the trapped volume of liposomes [34]. The calcein content in W/O/W emulsions was determined from the fluorescence intensity before and after cobalt(II) ions were added, which quench florescence of calcein by chelate formation. Fluorescence intensity was measured with a fluorescence spectrophotometer (FP-777; JASCO Co., Tokyo, Japan). The fluorescence intensity from 3 ml of W/O/W emulsions was measured before (F_{tot}) and after (F_{in}) addition of 30 μl of $CoCl_2$ (0.01 M). F_{tot} corresponds to the fluorescence from all materials composing the W/O/W emulsion. F_{in} corresponds to the fluorescence from the internal water phase plus the fluorescence from the W/O/W emulsion itself. The entrapment yield is calculated from the equation

$$\text{entrapment yield } (\%) = \frac{(F_{\mathrm{in}} - F_{\mathrm{wow}})}{(F_{\mathrm{tot}} - F_{\mathrm{wow}})} \times 100, \tag{2}$$

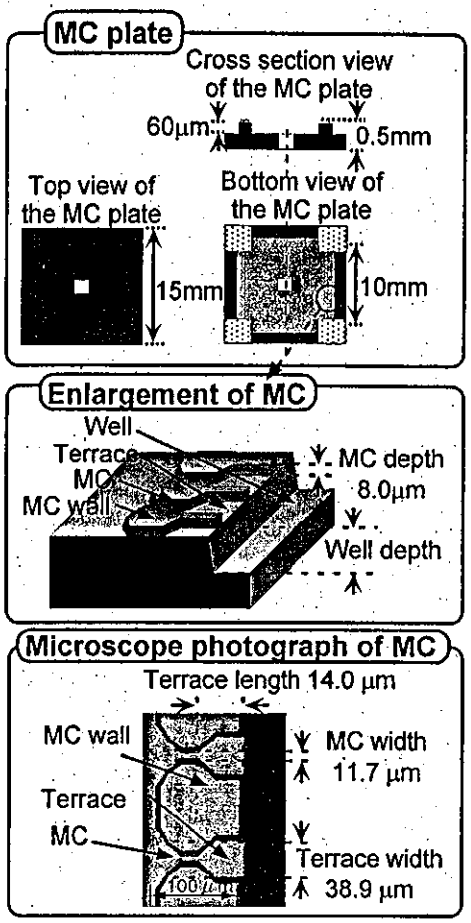

Fig. 2. Silicon MC plate.

where, F_{wow} represents the fluorescence intensity from the W/O/W emulsion itself, meaning the W/O/W emulsion without calcein, which was measured separately. The dilution from adding $CoCl_2$ solution can be neglected because of the small volume of the added solution. The entrapment yield calculated from Eq. (2) represents the ratio of the material amount entrapped in the internal water phase to the amount in the total recovered emulsion.

3. Results and discussion

3.1. Preparation of W/O/W emulsions using MC emulsification

First-step emulsification was performed with a homogenizer. Decane, ethyl oleate, MCT, and triolein were used as oil phases. Five percent of CR-310 was dissolved in each oil phase and used as the surfactant for W/O emulsion. Tris–HCl buffer was used for the internal water phases. The internal water phases were gently added to the oil phase by mixing with a homogenizer until the volume fraction of water phase reached 10%. The homogenizer rotation speed and mixing time were controlled as the premixed W/O emulsions have droplets with diameters ranging from 1 to 100 μm.

Table 1
Average diameters and coefficients of variation of the prepared W/O/W emulsions and the internal water droplets for four oil phases

Oil phase	Viscosity (mPa s)	$D_{a,\,W/O/W}$ (μm)	$CV_{W/O/W}$ (%)	$D_{a,\,W/O}$ (μm)	$CV_{W/O}$ (%)
Decane	1.3	32.6	5.5	21.0	26.8
Ethyl oleate	6.5	31.8	6.3	19.2	26.0
MCT	26	32.6	8.0	21.0	27.6
Triolein	69	35.7	19.0	17.9	29.6

CR-310 was used as a surfactant dissolved in oil phase. $D_{a,\,W/O/W}$ and $CV_{W/O/W}$ are the average diameter and the coefficient of variation for W/O/W emulsion. $D_{a,\,W/O}$ and $CV_{W/O}$ are the average diameter and the coefficient of variation for W/O emulsion.

Second-step emulsification was performed using MC emulsification, in which the premixed emulsions were pressurized into the external water phase. Tris–HCl buffer was used for the external water phase. The second-step MC emulsification was carried out at a W/O emulsion flow rate of 0.1 ml/h. In this case, no surfactant was added to the external water phase to avoid increasing its viscosity. Increased viscosity can lead to unsuccessful MC emulsification, especially for high-viscosity oil phases. Without surfactant in the external water phase, the prepared W/O/W emulsions were stable enough so that no coalescence was observed in the module. For long-time stability, a hydrophilic surfactant (high HLB) should be added after recovery of the W/O/W emulsion. Figure 3 shows the MC emulsification process observed through the microscope (DIC mode) using four oil phases. Figure 4 presents the prepared W/O/W emulsions observed through the microscope (DIC mode). Successful MC emulsification was observed for decane, ethyl oleate, and MCT, and monodispersed oil droplets containing small water droplets were prepared. MC emulsification was possible for triolein, but larger droplets were formed from some of the channels.

Figure 5 illustrates the droplet diameter distributions of the prepared W/O/W emulsions using four oil phases. D_a and CV of the W/O/W emulsions and the internal water droplets are shown in Table 1 for four oil phases. The internal water droplets, which were optically accessible (larger than 5 μm), were measured. Monodispersed oil droplets with CVs of 5 to 8% were prepared using decane, ethyl oleate, and MCT as oil phases. When the high-viscosity oil phases (MCT and triolein) were used, larger droplets formed and continuous outflow of the W/O emulsion phase occurred, resulting in a high CV of 19%.

In all cases, the droplet diameter distributions of the W/O/W emulsions were slightly wider than those in the previous study [29], where it was shown that the droplet diameter was affected by the viscosity ratio of the dispersed phase and the continuous phase [25]. If the dispersed phase is less viscous than the continuous phase, larger droplets are formed. The effective viscosity of a W/O emulsion, which corresponds to the dispersed phase in the second-step emulsification, is affected by the volume fraction of the internal water phase. During the MC emulsification, the volume

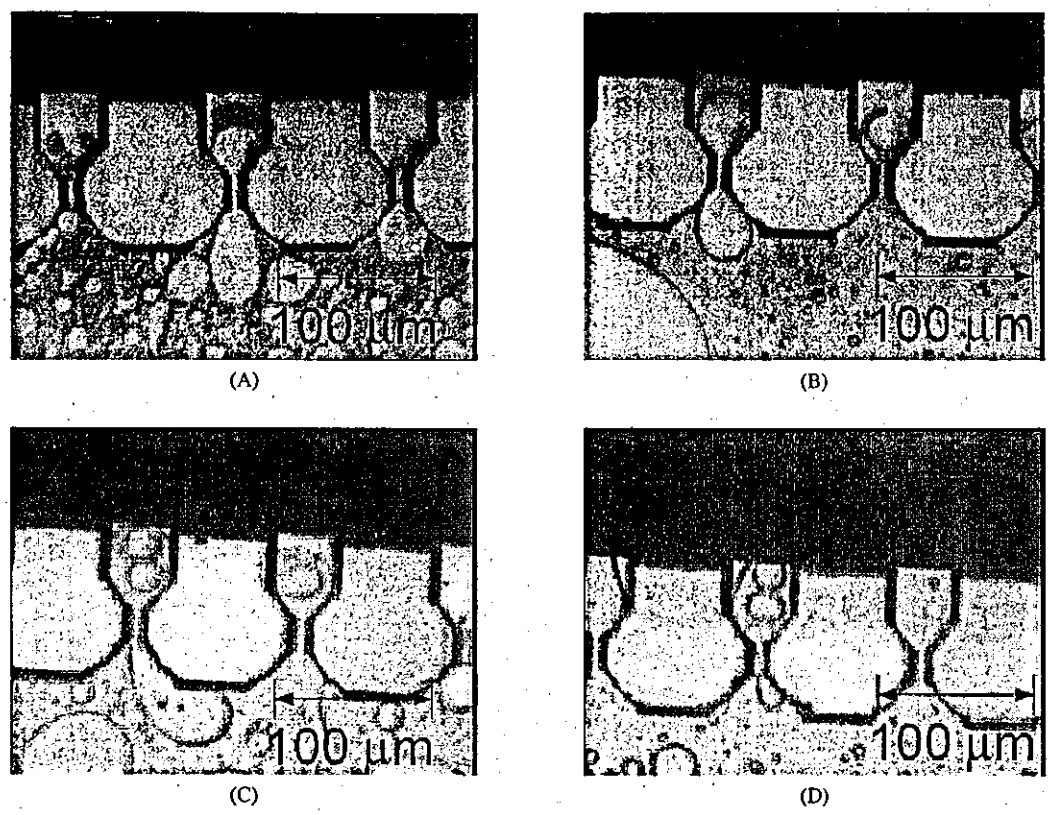

Fig. 3. Microscope photographs of MC emulsification process (DIC mode). Oil phases were decane (A), ethyl oleate (B), MCT (C), and triolein (D).

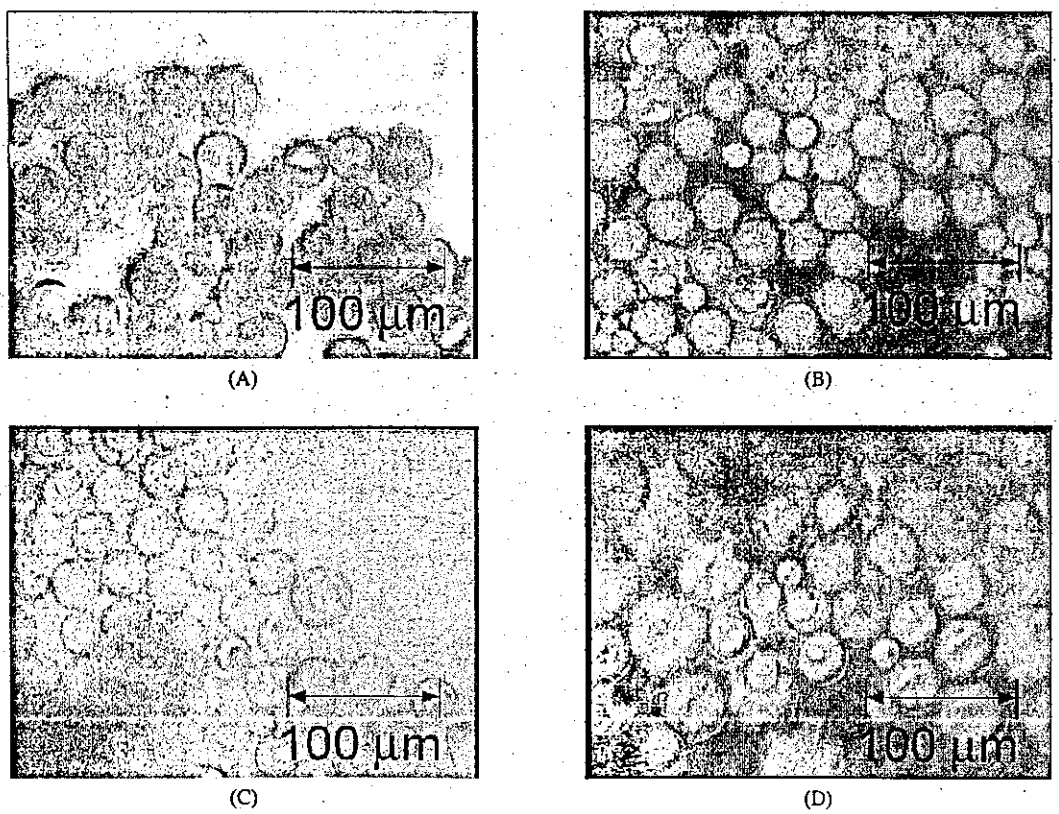

Fig. 4. Microscope photographs of prepared W/O/W emulsions (DIC mode). Oil phases were decane (A), ethyl oleate (B), MCT (C), and triolein (D).

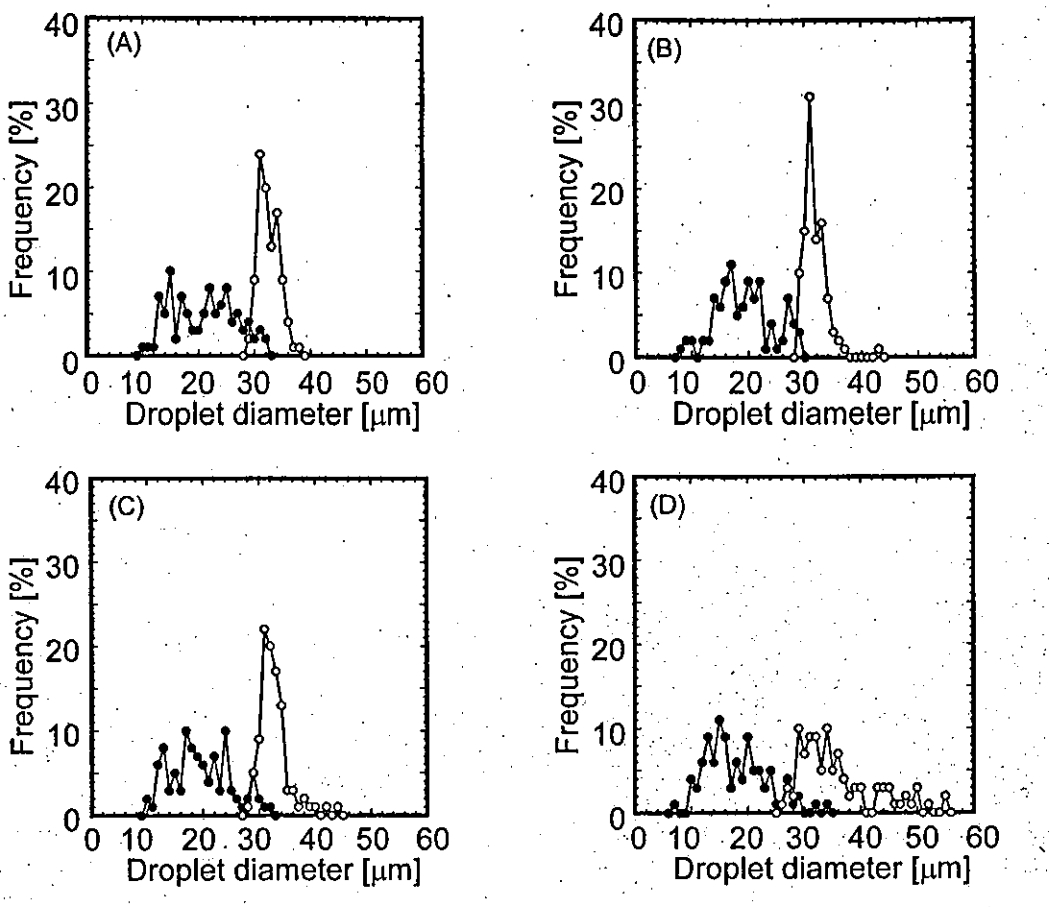

Fig. 5. Droplet diameter distributions of the prepared W/O/W emulsions (○) and internal water phases (●). Oil phases were decane (A), ethyl oleate (B), MCT (C), and triolein (D).

fractions of W/O emulsions penetrating the MC fluctuate because the premixed W/O emulsions do not have homogeneous structures on a microscopic scale. This leads to fluctuation in the viscosity of W/O emulsions and in the prepared droplet diameters. Consequently, the resulting W/O/W emulsions have larger CVs than those of the emulsions described in the previous study.

It is important to point out that no leakage of the internal water phase was observed optically during the MC emulsification process. Furthermore, no phase inversion or demulsification was observed during the MC emulsification process. The previous study reported phase inversion of the O/W emulsion produced using hydrophobic MC [35]. Hydrophilic membranes were also applied to disrupt the W/O emulsion [36]. Whether the dispersed phase is disrupted or penetrated may depend on the stabilization effect of the surfactant molecules added in the oil phases. The surfactant used in this study (CR-310) is known to effectively stabilize water droplets in oil and therefore could have prevented disruption of the thin oil film between the internal water phase and external water phase during MC emulsification. Interestingly, the thin oil film between the phases is strong enough that internal droplets larger than MCs also penetrated through the channel without disruption, as shown in Fig. 3. Internal water droplets larger than the resulting W/O/W droplets also penetrated through the channel and were divided into several droplets.

To investigate the behavior of the internal water droplets penetrating the MC, we studied the changes of the droplet diameters of the internal water phase after MC emulsification. We also investigated the size changes of the discrete internal water droplets and plotted the results in Fig. 6. For decane, ethyl oleate, and MCT, internal water droplets larger than the resulting W/O/W emulsion droplets were divided into almost the same size as the resulting W/O/W emulsion droplets (Figs. 3A and 3B). These W/O/W emulsions have larger internal droplets, which are almost the same size as the W/O/W emulsion droplets, and oil phases are like thin oil layers. These vesicle-like W/O/W emulsions were found in Figs. 4A, 4B, and 4C. In contrast, several smaller internal water droplets were entrapped into a single W/O/W emulsion droplet (Fig. 4). For MCT and triolein, internal water droplets larger than the resulting W/O/W emulsion droplets were sheared at the MC and divided into smaller droplets, as shown in Figs. 3C and 3D. The larger internal water droplets might have been sheared at the MC by the high-viscosity flow of MCT and triolein, and the sheared smaller droplets may have been entrapped in the W/O/W emulsion droplets during the detachment of W/O/W emulsion droplets. In all cases, the strong stabilizing effect of CR-310 and the mild

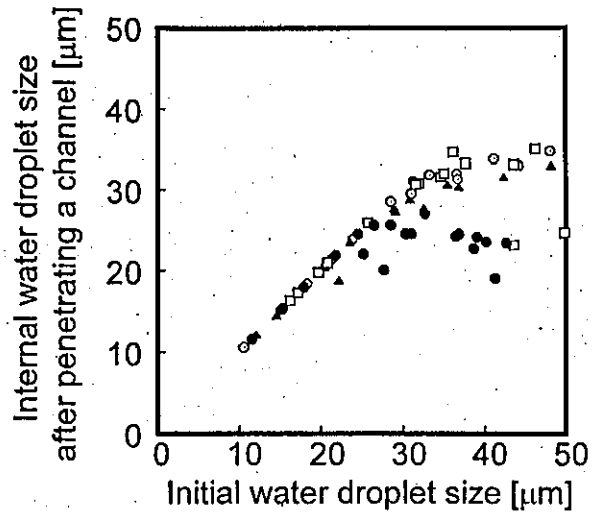

Fig. 6. Changes of the droplet diameter of internal water phase after MC emulsification. Oil phases were decane (○), ethyl oleate (▲), MCT (□), and triolein (●).

Table 2
Fluorescence intensities of calcein entrapped in W/O/W emulsion

No.	Sample	Fluorescence intensity (arbitrary units)
1	W/O/W emulsion containing calcein (F_{tot})	3650
2	W/O/W emulsion containing calcein + $CoCl_2$ (F_{in})	3393
3	W/O/W emulsion without calcein (F_{WOW})	735
4	Calcein in Tris–HCl buffer	2507
5	Calcein in Tris–HCl buffer + $CoCl_2$	1.58

The voltage applied to the photomultiplier was high-mode for samples 1, 2, and 3, and low-mode for samples 4 and 5.

droplet formation action of MC emulsification resulted in effective entrapment of the internal water phase without disruption.

3.2. Entrapment yield in W/O/W emulsion

We studied the entrapment yield fluorometrically using calcein solution. Tris–HCl buffer containing 4×10^{-4} M calcein was used as the internal water phase. MCT with 5% CR-310 was used as the oil phase. Tris–HCl buffer containing 1% PGML was used as the external water phase. The first-step emulsification was performed using a homogenizer at 5000 rpm for 3 min. The internal water phases were gently added to the oil phases by mixing with a homogenizer until the volume fraction of the water phase reached 10%. The second-step MC emulsification was conducted at a 0.1 ml/h W/O emulsion flow rate for 1 h. The prepared W/O/W emulsion was recovered by 100 ml of external water phase. The resulting oil-phase content in the external water phase was approximately 0.1%. The final calcein concentration was calculated to be approximately 4×10^{-8} M.

Figure 7 presents the prepared W/O/W emulsion observed using a microscope in DIC mode (Fig. 7A) and fluorescent mode (Fig. 7B). The fluorescent image shows

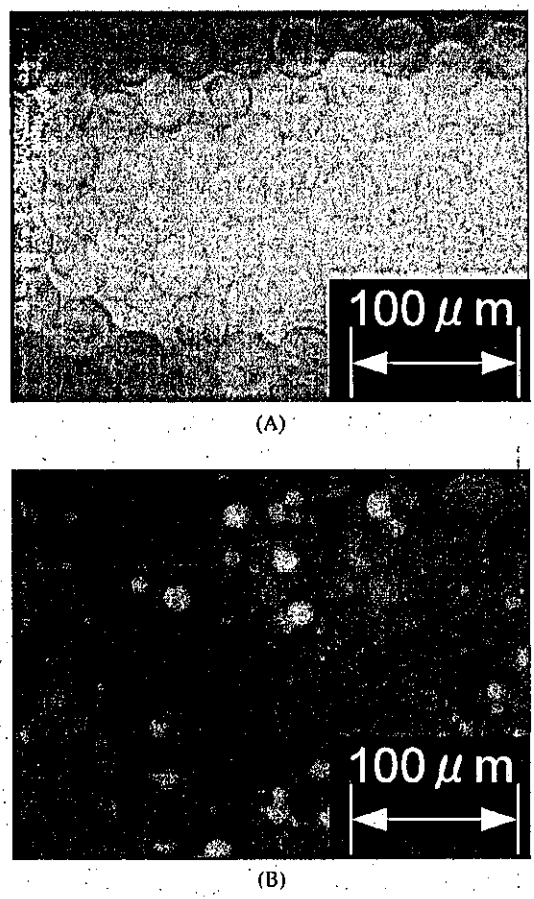

Fig. 7. Microscope photographs of the prepared W/O/W emulsion observed in DIC mode (A) and fluorescence mode (B).

the discrete internal water droplets inside the W/O/W emulsions. No fluorescence was observed outside the W/O/W emulsions, indicating a high entrapment yield. Table 2 lists the fluorescence intensities of calcein entrapped in W/O/W emulsions. The entrapment yield calculated by Eq. (2) was 91%. The mild action of droplet formation during MC emulsification led to high entrapment yields. The fluorescence from W/O/W emulsion itself is not negligible (Table 2, No. 3) but is corrected by Eq. (2). We conducted a control experiment in order to confirm the quenching ability of cobalt ions. The fluorescence of 3 ml of the 4×10^{-6} M calcein solution was measured before (Table 2, No. 4) and after (Table 2, No. 5) the addition of 30 μl of $CoCl_2$ (0.01 M). The control experiment revealed that the cobalt ion is a very efficient quencher of calcein fluorescence. The above results demonstrate that MC emulsification enables preparing W/O/W multiple emulsions with high entrapment yields because of its mild action during droplet formation.

We think that other methods, such as membrane emulsification and shear rupturing, also provide high entrapment yields. In particular, the shear-rupturing method provides high entrapment yields close to 98% [20]. Compared to the membrane emulsification method, MC emulsification has superior monodispersity. Using membrane emulsification, it is difficult to produce emulsions with a CV of less than 10%.

MC emulsification is more useful than the shear-rupturing method for producing emulsions with low viscosity oil and water phases. The shear rupturing method is applied only for highly viscous continuous phase because droplet formation is based on shear stress [20]. In regard to the droplet diameter range, MC emulsification produces larger emulsions (up to 100 μm [37]) than membrane emulsification (submicrometers to 60 μm [16]) and the shear-rupturing method (1 to 20 μm [20]). A disadvantage of MC emulsification is its low production rate. However, we believe MC emulsification can be scaled up by a factor of 10^3 to 10^4 compared with this study by using a larger MC plate, straight-through MC [24], and multiple MC plates.

4. Summary

MC emulsification was applied to prepare W/O/W emulsions using four oil phases. Successful MC emulsification was observed for decane, ethyl oleate, and MCT, and monodispersed oil droplets containing small water droplets were prepared. MC emulsification was possible for triolein, but larger droplets were formed from some of the channels. In all cases, the droplet diameter distributions of the W/O/W emulsion were slightly wider than those in the previous study because the viscosity of the premixed W/O emulsions fluctuated due to the non-homogeneous structure of the W/O emulsions. No leakage of the internal water phase was observed during the MC emulsification process. Furthermore, internal droplets larger than the MC also penetrated through the channel without disrupting the thin oil film. For decane, ethyl oleate, and MCT, internal water droplets larger than the resulting W/O/W emulsion droplets were divided into almost the same size as the resulting W/O/W emulsion droplets. For MCT and triolein, internal water droplets larger than the resulting W/O/W emulsion droplets were sheared at the MC and divided into smaller droplets. The entrapment yield in a W/O/W emulsion was measured fluorometrically and determined to be 91%. MC emulsification has the advantage of a high entrapment yield, resulting from mild action during droplet formation.

Acknowledgments

We thank Dr. K. Nagayama (Kochi National College of Technology) for his advice on our experimental system. We also thank Taiyo Kagaku Co. Ltd. for providing MCT and Sakamoto Yakuhin Kogyo Co. Ltd. for providing glycerin condensed ricinoleic acid esters and polyglycerin fatty acid esters. This work was supported by MAFF, Program for Nanotechnology Project, and the Program for Promotion of Fundamental Studies in Health Sciences of the Organization for Pharmaceutical Safety and Research of Japan.

References

[1] W. Seifriz, J. Phys. Chem. 29 (1925) 738.
[2] P. Sherman (Ed.), Emulsion Science, Academic Press, New York, 1968, p. 206.
[3] S. Matsumoto, J. Colloid Interface Sci. 94 (1983) 362.
[4] P. Becher, J. Soc. Cosmetic Chem. 9 (1958) 141.
[5] S. Matsumoto, Y. Kita, D. Yonezawa, J. Colloid Interface Sci. 57 (1976) 353.
[6] H. Okochi, M. Nakano, Chem. Pharm. Bull. 44 (1996) 180.
[7] J.A. Omotosho, A.T. Florence, T.L. Whateley, Int. J. Pharm. 61 (1990) 51.
[8] A.T. Florence, D. Whitehill, J. Pharm. 11 (1982) 277.
[9] M.F. Ficheux, L. Bonakdar, F. Leal-Calderon, J. Bibette, Langmuir 14 (1998) 2702.
[10] N. Garti, Colloids Surf. A 123–124 (1997) 233.
[11] W. Hou, K.D. Papadopoulos, Chem. Eng. Sci. 51 (1996) 5043.
[12] A.T. Florence, D. Whitehill, J. Colloid Interface Sci. 79 (1981) 243.
[13] J. Bibette, D. Roux, F. Nallet, Phys. Rev. Lett. 65 (1990) 2470.
[14] J. Bibette, J. Colloid Interface Sci. 147 (1991) 474.
[15] T. Nakashima, M. Shimizu, M. Kukizaki, Key Eng. Mater. 61/62 (1991) 513.
[16] T. Nakashima, M. Shimizu, M. Kukizaki, Adv. Drug Deliv. Rev. 45 (2000) 47.
[17] Y. Mine, M. Shimizu, T. Nakashima, Colloids Surf. B 6 (1996) 261.
[18] S. Higashi, M. Shimizu, T. Nakashima, K. Iwata, F. Uchiyama, S. Tateno, S. Tamura, T. Setoguchi, Cancer 75 (1995) 1245.
[19] T.G. Mason, J. Bibette, Langmuir 13 (1997) 4600.
[20] C. Goubault, K. Pays, D. Olea, P. Gorria, J. Bibette, V. Schmitt, F. Leal-Calderon, Langmuir 17 (2001) 5184.
[21] T. Kawakatsu, Y. Kikuchi, M. Nakajima, J. Am. Oil Chem. Soc. 74 (1997) 317.
[22] T. Kawakatsu, G. Trägårdh, Y. Kikuchi, M. Nakajima, H. Komori, T. Yonemoto, J. Surfact. Deterg. 3 (2000) 295.
[23] S. Sugiura, M. Nakajima, M. Seki, Langmuir 18 (2002) 3854.
[24] I. Kobayashi, M. Nakajima, K. Chun, Y. Kikuchi, H. Fujita, AIChE J. 48 (2002) 1639.
[25] T. Kawakatsu, G. Trägårdh, C. Trägårdh, M. Nakajima, N. Oda, T. Yonemoto, Colloids Surf. A 179 (2001) 29.
[26] S. Sugiura, M. Nakajima, H. Ushijima, K. Yamamoto, M. Seki, J. Chem. Eng. Jpn. 34 (2001) 757.
[27] S. Sugiura, M. Nakajima, J. Tong, H. Nabetani, M. Seki, J. Colloid Interface Sci. 227 (2000) 95.
[28] S. Sugiura, M. Nakajima, H. Itou, M. Seki, Macromol. Rapid Commun. 22 (2001) 773.
[29] S. Sugiura, M. Nakajima, S. Iwamoto, M. Seki, Langmuir 17 (2001) 5562.
[30] J. Eggers, Rev. Mod. Phys. 69 (1997) 865.
[31] S. Sugiura, M. Nakajima, M. Seki, Langmuir 18 (2002) 5708.
[32] S. Sugiura, M. Nakajima, N. Kumazawa, S. Iwamoto, M. Seki, J. Phys. Chem. B 106 (2002) 9405.
[33] Y. Kikuchi, K. Sato, H. Ohki, T. Kaneko, Microvascular Res. 44 (1992) 226.
[34] N. Oku, D.A. Kendall, R.C. Macdonald, Biochim. Biophys. Acta 691 (1982) 332.
[35] T. Kawakatsu, R.M. Boom, H. Nabetani, Y. Kikuchi, M. Nakajima, AIChE J. 45 (1999) 967.
[36] J.T.F. Keurentjes, G.I. Doonbusch, K.V. Riet, Sep. Sci. Technol. 26 (1991) 409.
[37] S. Sugiura, M. Nakajima, N. Kumazawa, M. Seki, J. Am. Oil Chem. Soc. 79 (2002) 515.

Original Paper

Hepatic Arterial Infusion of 5-Fluorouracil and Extrabeam Radiotherapy for Liver Metastases from Pancreatic Carcinoma

Hiroshi Ishii, Junji Furuse, Michitaka Nagase, Masahiro Yoshino
Mitsuhiko Kawashima[1], Mitsuo Satake[1], Takashi Ogino[1], Hiroshi Ikeda[1]
Division of Hepatobiliary Pancreatic Medical Oncology and [1]Department of Radiology
National Cancer Center Hospital East, Kashiwa, Japan
Corresponding Author: Hiroshi Ishii MD, National Cancer Center Hospital East, 6-5-1 Kashiwanoha, Kashiwa, Chiba 277-8577, Japan
Tel: +81 471 33 1111, Fax: +81 471 31 4724, E-mail: hirishii@east.ncc.go.jp

ABSTRACT

Background/Aims: To examine the efficacy and safety of a combined modality therapy consisting of hepatic arterial infusion of 5-fluorouracil and external-beam radiotherapy in patients with advanced pancreatic carcinoma.

Methodology: Hepatic arterial infusion chemotherapy consisted of 5-FU 1000mg/m^2 administrated as a 5-hr continuous infusion once weekly. External-beam radiotherapy (total dose, 50Gy; 2Gy/day) was delivered to the pancreas tumor concurrently for 5-6 weeks. Seventeen patients with no distant metastases except to the liver were enrolled in this study.

Results: Patients received a median of 13 cycles of chemotherapy. Sixteen of 17 patients received a total radiotherapy dose of 50Gy. In one patient, treatment was discontinued after 24Gy of radiotherapy and 2 cycles of chemotherapy because of progressive disease. Nausea and vomiting were the most common types of toxicity. Grade 3 or worse toxicity was observed in 2 patients. Four patients developed gastroduodenal ulcers. Of the 16 patients, 7 (41%) showed a partial response, and 9 (53%) showed no change. The median overall survival was 4.5 months and 1-yr overall survival of 11.8% was observed.

Conclusions: The combined therapy is active and well tolerated, but results in a poorer prognosis, in spite of its high initial response rate.

KEY WORDS: Pancreatic carcinoma; Liver metastasis; Hepatic arterial infusion; 5-fluorouracil; Radiotherapy

ABBREVIATIONS: Hepatic Arterial Infusion (HAI); External-Beam Radiotherapy (EBRT); 5-fluorouracil (5-FU); Partial Response (PR); No Change (NC); Progressive Disease (PD); Carbohydrate Antigen 19-9 (CA19-9); Computed Tomography (CT); World Health Organization (WHO)

INTRODUCTION

Liver metastasis is a common progression of pancreatic carcinoma and the prognosis of patients in whom it occurs is extremely poor. Although gemcitabine has been shown to be an active agent in the treatment of advanced pancreatic carcinoma, it has not been observed to adequately prolong patient survival (1). Hepatic arterial infusion (HAI) of 5-fluorouracil (5-FU) has been performed in several clinical trials in patients with liver metastasis from colorectal cancer and the findings indicate that HAI results in a high response rate (2,3). In addition, with regard to pancreatic carcinoma, recent study of HAI chemotherapy after vascular supply distribution via superselective embolization has also demonstrated promising results (4). At the present time, combined external-beam radiation therapy (EBRT) and 5-FU therapy are considered standard treatment for locally advanced pancreatic carcinoma (5-7). Thus, EBRT combined with HAI therapy using 5-FU is thought to have high clinical applicability and may prove beneficial to patients with pancreatic carcinoma without distant metastases, except to the liver. We therefore conducted a phase 2 study of combined EBRT and HAI using 5-FU to clarify the efficacy and safety of this treatment in patients with pancreatic carcinoma with metastasis restricted to the liver.

METHODOLOGY

Seventeen patients with advanced pancreatic cancer complicated by liver metastasis underwent HAI chemotherapy and EBRT between February 1998 and November 2000 at the National Cancer Center Hospital East. The eligibility criteria for inclusion in this study were: 1) histological proof of adenocarcinoma of the pancreas, 2) no distant metastases on computed tomography (CT) staging, except to the liver, 3) no previous anti-cancer treatment, 4) a performance status of 0, 1, or 2 according to the World Health Organization (WHO) grading system (8), 5) adequate bone marrow functioning (blood cell count of 4,000 or greater, platelet count of 100,000 or greater, and hemoglobin of 10g/dL or greater), adequate renal function (serum creatinine level of less than 1.1mg/dL), and adequate hepatic function (serum bilirubin level of less than 3.0mg/dL, serum alanine and aspartate transaminase levels of less than 200 IU/L), 6) no serious complications, and 7) receipt of written informed consent from the patient. Percutaneous biliary drainage was performed in patients with obstructive jaundice, and patients were required to have a total serum bilirubin level of less than 3.0mg/dL before initiation of treatment. Patient characteristics are summarized in **Table 1**.

Hepatic arteriography was performed prior to

Hepato-Gastroenterology 2004; 51:1175-1178

TABLE 1 Patient Characteristics

Characteristic	No. of patients (%)
Gender	
Male	11 (65%)
Female	6 (35%)
Median age (range)	59 (50-77)
WHO performance status	
0	5 (29%)
1	10 (59%)
2	2 (12%)
Location of primary tumor	
Head	5 (29%)
Body/tail	12 (71%)
Median CEA, ng/mL (range)	8.6 (0.8-185)
Median CA 19-9, U/mL (range)	827 (21-14552)

WHO: World Health Organization;
CEA: carcinoembryonic antigen;
CA 19-9: carbohydrate antigen 19-9.

catheter placement to determine the degree of arterial blood supply to the liver. The gastroduodenal and right gastric arteries of all patients were ligated with steel coils to prevent drug perfusion into the stomach and the duodenum. A catheter was positioned in the gastroduodenal artery. Catheters were placed via the left subclavian artery. The port was connected to the catheter and implanted in the subcutaneous space of the left chest wall.

After implanting the catheter and the port, 5-FU (1,000mg/m^2) mixed with 100mg of hydrocortisone (Solu-Cortef; Pharmacia & Upjohn, New Jersey, USA) and 5,000 U of heparin, was administrated over 5 hours through a battery-operated ambulatory infusion pump. After drug infusion, 20mL of saline and 5,000 U of heparin were infused through the pump. Cycles of intra-arterial infusion were repeated once weekly, unless there was evidence of disease progression or unacceptable toxicity levels.

Radiation therapy was delivered using the conformal, arc rotation technique to deliver a 10-MV X-ray, in order to achieve a total dose of 50Gy, given in 25 fractions over 5 weeks. The radiation field included the primary tumor and a 1- to 3-cm margin which covered the pancreaticoduodenal and celiac axis lymph nodes. This field was defined during treatment-planning CT one or two days before radiation therapy.

The toxicity of treatment was scored weekly according to WHO criteria (8). Both radiotherapy and chemotherapy were suspended if grade 3 toxicity was encountered, and resumed upon recovery to a grade 2 level of toxicity.

Follow-up CT was performed every month for 6 months, and every 2 months thereafter, in order to assess objective tumor responses according to WHO criteria. Local progression was diagnosed when the primary tumor was enlarged on CT, or when obstructive jaundice occurred after treatment. Overall survival was measured from the first day of treatment, and the survival rate was calculated by the Kaplan-Meier method (9). Serum CA 19-9 levels were measured every month by immunoradiometric assay using the Centocor radioimmunoassay kit (Centocor, Inc., Malvern, PA).

Patients received a full explanation about this study and gave written informed consent after approval of the protocols by the Institutional Review Board of the National Cancer Center.

RESULTS

A total of 251+ cycles of HAI chemotherapy were administrated (median 13, range 2-34+). Of 17 patients, 16 received EBRT with a total dose of 50Gy. In the remaining patient, treatment was discontinued after receipt of 24Gy of EBRT and 2 cycles of HAI because of disease progression. Therapy was discontinued due to disease progression in 14 patients, hepatic arterial obstruction in 1, and duodenal ulcer in 1. One patient was still receiving HAI chemotherapy at the time of writing.

Manifestations of treatment-related toxicity are summarized in **Table 2**. No life-threatening toxicity was observed, but 2 patients (12%) encountered Grade 3 toxicity. Nausea and vomiting were the most common types of toxicity. Four patients developed gastroduodenal ulcers after EBRT. Of these patients, one required hospitalization due to bleeding, and another

TABLE 2 Treatment-Related Toxicity according to WHO Criteria

	No. of patients (%)	
	Grade	
Toxicity	2	3
Leucopenia	3 (18%)	0
Anemia	0	0
Thrombocytopenia	3 (18%)	0
Nausea/vomiting	6 (35%)	2 (12%)
Liver dysfunction	0	0
Diarrhea	0	0
Mucositis	0	0

WHO: World Health Organization.

TABLE 3 Changes in the CA 19-9 levels of Patients with Elevated CA 19-9 Levels after Treatment (>100 U/mL)

Case no.	CA 19-9 (U/mL) Before *	After #	Tumor response$	Survival (days)
1	14552		NC	80
2	13216		PD	35
3	9945		PR	84
4	3944	673	PR	402
5	3091	292	NC	86
6	1739	53	PR	349
7	1526		NC	136
8	1428		NC	133
9	827		NC	114
10	318		PR	264
11	212		NC	114
12	170	41	NC	234

CA 19-9: carbohydrate antigen 19-9, NC: no change, PR: partial response, PD: progressive disease. *Maximal levels before treatment are represented; #Minimal levels after treatment are represented where responses were observed; $Assessed by computed tomography.

TABLE 4 Patterns of Initial Disease Progression

	No. of patients
Peritoneum (ascites)	6
Peritoneum and lymph node	1
Liver	2
Liver and lymph node	1
Liver and bone	1
Lymph node	1
Bone	1

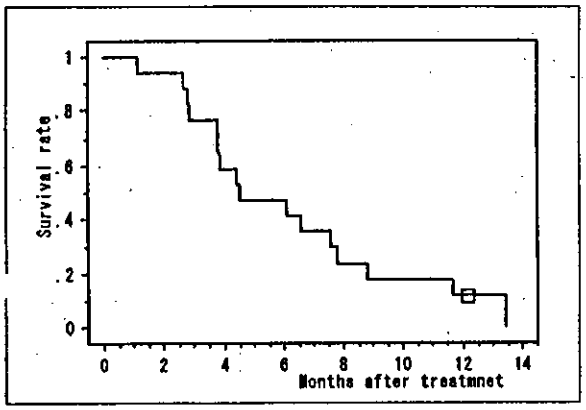

FIGURE 1 Overall survival curve for 17 patients treated with radiation and hepatic arterial 5-fluorouracil infusion. An open square indicates a censored case.

discontinued HAI therapy because of a refractory duodenal ulcer 5 months after initiation of treatment.

Seven (41%) patients had partial responses, 9 (53%) remained stable, and one showed progressive disease. Serum CA 19-9 levels were reduced by more than 50% in 4 of 12 patients (33%) who had pretreatment CA 19-9 levels of 100 U/mL or greater (**Table 3**). Death from cancer was documented in 16 patients at the time of analysis. The initial sites of disease progression were documented in 13 patients (**Table 4**). Peritoneal dissemination was the main cause of progression. Overall survival curves are shown in **Figure 1**. The median overall survival was 4.5 months and 1-yr overall survival was 11.8% observed.

DISCUSSION

Systemic chemotherapy using gemcitabine is considered standard therapy for advanced pancreatic carcinoma. However, a tumor response rate of only 5.4% and a survival time of 5.65 months have been observed with gemcitabine treatment, neither of which are satisfactory outcomes (1). High response rates of liver metastasis to HAI in patients with colorectal carcinoma have been reported (2,3,10). In a previous study (10), we employed continuous HAI of 5-FU for 5 days at a dose of 500mg/m^2/day every 4 weeks in order to treat liver metastasis from pancreatic carcinoma. The treatment was feasible but the overall response rate was only 8% at this dose and schedule. For treatment of liver metastasis from colorectal carcinoma, Arai *et al.* (3) reported a response rate of 78% after intermittent HAI of high-dose 5-FU once a week on an outpatient basis. In accordance with phase 1 and 2 studies, we therefore tried weekly HAI of 5-FU at a dose of 1000mg/m^2 for treatment of isolated liver metastasis from pancreatic carcinoma.

The toxicity associated with this regimen seemed to be mild. In the current study, grade 4 toxicity was not observed and the percentage of patients with grade 3 or worse toxicity was low (12%). Throughout the course of treatment, hematological toxicity was frequent but mild, and gastrointestinal toxicity was the only cause of treatment interruption. In a previous pilot study (11), hepatic artery occlusion was observed in 23% of patients and was the second cause of treatment discontinuation. However, occlusion of the hepatic artery occurred in only one patient (6%) in the current study. The frequency of hepatic artery thrombosis due to 5-FU infusion seemed to be lower with use of the intermittent schedule. On the other hand, gastroduodenal ulcers were frequently observed (24%), compared to a previous study in which HAI was administered continuously (8%) (11).

In the current study, an objective tumor response of 41% was noted following CT assessment. Serum CA 19-9 levels were reduced in 33% of patients with high initial CA 19-9 levels. Nine of the patients (53%) responded to therapy, as evaluated by CT or measurement of CA 19-9 levels. Greater response rates were observed with combination therapy than with any other form of systemic chemotherapy in the treatment of advanced pancreatic carcinoma. However, high response rates did not translate into prolonged survival for the patients in this study. For example, one of the patients who responded to treatment died due to peritoneal dissemination only 2.8 months after the initiation of the treatment. As shown in **Table 4**, peritoneal dissemination was the major cause of treatment failure. Hepatic extraction of 5-FU after HAI was estimated to be between 15-50% (12), thus, we expected a 150-500mg/m^2 weekly dose of 5-FU to produce a systemic anti-tumor effect. However, this dose seemed insufficient to reduce distant metastases, especially peritoneal dissemination. Surgical exploration revealed minute peritoneal metastasis in 12.5% of patients who had no distant metastases but locally unresectable pancreatic carcinoma, as assessed by CT staging (13).

Recently, excellent results have been reported using arterial infusion chemotherapy at the primary site of pancreatic carcinoma (4,14). In these reports, regional chemotherapy for pancreatic carcinoma was repeated for as long as catheters remained patent without occlusion or dislocation. Long-term tumor control might be obtained via this method, provided the tumor is responsive to the agent being infused. With respect to radiotherapy, however, it would be difficult to deliver a dose exceeding 72Gy to the pancreatic region, regardless of whether or not the tumor is responsive to radiotherapy (15). We will not select a higher dose of EBRT in combination with HAI in our next trial because we do not believe intensification of radiotherapy can reduce distant progression in pancreatic cancer patients. We do not know whether regional chemotherapy has the ability to reduce peri-

toneal dissemination from pancreatic carcinoma. However, this might explain the prolonged survival of patients in studies involving regional chemotherapy (4,14).

We conclude that liver metastasis from pancreatic cancer responds well to HAI, but that combination therapy fails to prolong the survival of such patients. Thus, we do not feel that a radiotherapeutic approach can be used to treat patients with pancreatic carcinoma who do not have distant metastases, except to the liver, as evaluated by clinical staging. Therefore, HAI should be used in combination with either systemic chemotherapy or regional chemotherapy at the primary site.

REFERENCES

1 **Burris HA 3rd, Moore MJ, Andersen J, Green MR, Rothenberg ML, Modiano MR, Cripps MC, Portenoy RK, Storniolo AM, Tarassoff P, Nelson R, Dorr FA, Stephens CD, Von Hoff DD:** Improvements in survival and clinical benefit with gemcitabine as first-line therapy for patients with advanced pancreatic cancer: a randomized trial. J Clin Oncol 1997; 15:2403-2413.

2 **Sugihara K:** Continuous hepatic arterial infusion of 5-fluorouracil for unresectable colorectal liver metastases: phase 2 study. Surgery 1995; 117:624-628.

3 **Arai Y, Inaba Y, Takeuchi Y, Ariyoshi Y:** Intermittent hepatic arterial infusion of high-dose 5FU on a weekly schedule for liver metastases from colorectal cancer. Cancer Chemother Pharmacol 1997; 40:526-530.

4 **Homma H, Doi T, Mezawa S, Takada K, Kukitsu T, Oku T, Akiyama T, Kusakabe T, Miyanishi K, Niitsu Y:** A novel arterial infusion chemotherapy for the treatment of patients with advanced pancreatic carcinoma after vascular supply distribution via superselective embolization. Cancer 2000; 89:303-313.

5 **Moertel CG, Childs DS, Reitemeier RJ, Colby MY, Holbrook MA:** Combined 5-fluorourail and supervoltage radiation therapy of locally unresectable gastrointestinal cancer. Lancet 1969; 2:865-867.

6 **The Gastrointestinal Tumor Study Group:** Therapy of locally unresectable pancreatic carcinoma: a randomized comparison of high dose (6000 rads) radiation alone, moderate dose radiation (4000 rads + 5-fluorouracil), and high dose radiation + 5-fluorouracil. Cancer 1981; 48:1705-1710.

7 **Gastrointestinal Tumor Study Group:** Treatment of locally unresectable carcinoma of the pancreas: comparison of combined-modality therapy (chemotherapy plus radiotherapy) to chemotherapy alone. J Natl Cancer Inst 1988; 80:751-755.

8 **World Health Organization:** WHO Handbook for Reporting Results of Cancer Treatment. offset publication 48. Geneva, World Health Organization, 1979.

9 **Kaplan EL, Meier P:** Nonparametric estimation from incomplete observations. J Am Stat Assoc 1958; 63:457-481.

10 **Harmantas A, Rotstein L, Langer B:** Regional versus systemic chemotherapy in the treatment of colorectal carcinoma metastatic to the liver. Is there a survival difference? Meta-analysis of the published literature. Cancer 1996; 78:1639-1645.

11 **Furuse J, Maru Y, Yoshino M, Mera K, Sumi H, Tajiri H, Satake M, Onaya H, Ishikura S, Ogino T, Kawashima M, Ikeda H:** Hepatic arterial infusion of 5-fluorouracil for liver metastases from pancreatic carcinoma: results from a pilot study. Hepatogastroenterology 2001 48:208-211.

12 **Collins JM:** Pharmacologic rationale for regional drug delivery. J Clin Oncol 1984; 2:498-504.

13 **Furuse J, Ogino T, Ryu M, Kinoshita T, Konishi M, Kawano N, Ishikura S, Shimizu W, Sekiguchi R, Moriyama N, Iwasaki M, Yoshino M:** Intraoperative and conformal external beam radiation therapy in patients with locally advanced pancreatic carcinoma; results from a feasibility phase II study. Hepatogastroenterology 2000; 47:1142-1146.

14 **Ohigashi H, Ishikawa O, Imaoka S, Sasaki Y, Kabuto T, Kameyama M, Furukawa H, Hiratuka M, Nakamori S, Nakano H, Yasuda T, Iwanaga T:** A new method of intra-arterial regional chemotherapy with more selective drug delivery for locally advanced pancreatic cancer. Hepatogastroenterology 1996; 43:338-345.

15 **Ceha HM, van Tienhoven G, Gouma DJ, Veenhof CHN, Schneider CJ, Rauws EAJ, Phoa SSKS, Gonzalez DG:** Feasibility and efficacy of high dose conformal radiotherapy for patients with locally advanced pancreatic carcinoma. Cancer 2000; 89:2222-2229.

Synovial Sarcoma of the Soft Tissues

Prognostic Significance of Imaging Features

Ukihide Tateishi, MD, PhD, Tadashi Hasegawa, MD, PhD, Yasuo Beppu, MD, Mitsuo Satake, MD, and Noriyuki Moriyama, MD, PhD

Objective: This study assessed the prognostic value of computed tomography (CT) and magnetic resonance (MR) imaging features in synovial sarcoma of the soft tissues.

Methods: CT and MR imaging studies were performed in 30 patients with pathologically confirmed synovial sarcoma of the soft tissues. CT and MR imaging findings obtained by 2 radiologists with agreement by consensus were compared for histopathologic features including tumor grade. Univariate analyses were conducted to clarify the impact of imaging findings on overall survival with a medium duration of 32 months. Multivariate analysis was estimated using a Cox proportional hazards model with the relative risk of each variable.

Results: Statistically significant imaging findings favoring a diagnosis of high-grade tumor included proximal distribution ($P < 0.01$), large tumor size (>10 cm, $P < 0.05$), the absence of calcification ($P < 0.05$), tumor possessing cyst ($P < 0.01$), the presence of hemorrhage ($P < 0.05$), and the presence of triple signal pattern ($P < 0.05$). Univariate analysis showed that proximal distribution ($P < 0.05$), tumor size larger than 5 cm ($P < 0.01$), the absence of calcification ($P < 0.01$), the presence of hemorrhage ($P < 0.05$), and the presence of triple signal pattern ($P < 0.05$) had a significant association with the disease-free survival (DFS). Multiple logistic regression models revealed that tumor size larger than 10 cm had a significant impact on the DFS with relative risk of 18.8 ($P < 0.05$).

Conclusion: CT and MR imaging studies allow prognosis prediction in patients with synovial sarcoma of the soft tissues.

Key Words: computed tomography, magnetic resonance imaging, synovial sarcoma

(*J Comput Assist Tomogr* 2004;28:140–148)

From the Divisions of Diagnostic Radiology (Drs Tateishi, Satake, and Moriyama), Pathology (Dr Hasegawa), and Orthopedics (Dr Beppu), National Cancer Center Hospital and Research Institute, Tokyo, Japan.

This work was carried out by the Program for Promotion of Fundamental Studies in Health Sciences of the Organization for Pharmaceutical Safety and Research (Japan) and was supported in part by a Grant-in-Aid for Cancer Research from the Ministry of Health, Labor and Welfare.

Reprints: Ukihide Tateishi, MD, PhD, Division of Diagnostic Radiology, National Cancer Center Hospital, 5-1-1, Tsukiji, Chuo-Ku, Tokyo 104-0045, Japan (e-mail: utateish@ncc.go.jp).

Synovial sarcoma is the fourth most common soft tissue sarcoma, comprising 10% of all soft tissue sarcomas and arising most frequently in the extremities, generally in the vicinity of the joints, bursae, and tendon sheaths.[1–3] Synovial sarcoma is a morphologically high-grade sarcoma that has been extensively described.[4–6] However, some patients develop metastases quite early after surgery and die of disease whereas a distinct group of patients have prolonged courses without recurrence or metastasis. For these reasons, it is imperative that accurate tumor grading should be made to determine the prognoses for patients in synovial sarcoma of the soft tissues.

Several studies showed that the characteristic features in synovial sarcoma of the soft tissues are nonspecific and attributable mainly to heterogeneity which includes necrosis, calcification, and hemorrhage.[7–18] Tumors appear on T2-weighted MR images as soft tissue masses of marked heterogeneity often associated with various degrees of internal septa.[8–12] However, the relationships between these imaging features and the prognoses for patients were not fully understood. We undertook this retrospective study in a series of patients with synovial sarcoma of the soft tissues to assess the prognostic value of computed tomography (CT) and magnetic resonance (MR) imaging features.

PATIENTS AND METHODS

Patients

We reviewed the cases of 30 patients with synovial sarcoma of the soft tissues who were registered in our pathology files. The clinical details, including follow-up information, were obtained by reviewing all the medical charts. Eighteen (60%) of the 30 patients were female and 12 (40%) were male. Their median age at diagnosis was 27 years and ranged from 10 to 61 years. No patients were lost to follow-up, which began on the date of primary surgery. The median duration of follow-up was 32 months and ranged from 0 to 95 months. Disease-free survival (DFS) was recorded as the time from diagnosis to death due to any cause. Both metastasis-free survival (MFS) and recurrence-free survival (RFS) were also calculated.

An expert pathologist, who had developed the tumor grading system that we used, reviewed for diagnosis the histo-

logic slides of all the tumors of patients. Immunohistochemical staining was carried out in all patients to confirm the diagnosis or tumor type according to the classification system described by Enzinger and Weiss.[3] Histologically, 14 tumors (47%) were classified as monophasic fibrous subtype, 11 (37%) as biphasic, and 5 (17%) as poorly differentiated. In this study, the histological grade of each tumor was determined using a grading system established by Hasegawa et al.[19–21] According to this grading system, synovial sarcomas were assigned low- or high-grade: low-grade, n = 6 (20%); high-grade, n = 24 (80%). Excised specimens were available for review or for mapping correlation with images.

Imaging Studies

Images reviewed included CT scans (all with pre- and postcontrast enhancement) and MR images (in all patients with contrast enhancement). CT scanning was performed with 1 of 2 models in all patients (Aquilion V-detector CT scanner or X-Vigor helical CT scanner, Toshiba Medical Systems, Tokyo, Japan). On average, initial CT scans and MR examinations on all patients were performed within 10 days. Scanning parameters for CT scans were axial single or 4-slice mode, 4.0-mm section thickness, 0.5 or 1.0 seconds/rotation, 120–150 kVp, and 200–250 mA. Images were reconstructed at 10.0-mm slice thickness using a standard algorithm without edge enhancement. MR imaging was performed using 1 of 2 models of 1.5-T systems (General Electric Medical Systems, Milwaukee, WI, or Toshiba Medical Systems, Tokyo, Japan). T1-weighted spin-echo MR images (TR/TE: 400 to 750/8 to 17 milliseconds) were obtained in the transverse plane using a dedicated body or surface coil. Using the spin-echo or fast spin-echo technique, T2-weighted images (TR/TE_{eff}: 2000 to 7000/117 to 144 milliseconds; 12–16 echo train) were then obtained in transverse and coronal planes. The images were obtained with a field of view of 16–26 cm, an image matrix of 128 × 160 to 256, a slice thickness of 4–10 mm, 0.4–1.0 mm gap, and 1–4 signals acquired. Postcontrast fat-saturated T1-weighted images were obtained in transverse and coronal planes after the intravenous administration of 0.1 mmol/kg of gadopentetate dimeglumine (Magnevist; Nihon-Shering, Osaka, Japan).

Image Analysis

All CT and MR images were reviewed by 2 radiologists and the findings were reported as a consensus opinion. The lesions were judged according to the characteristics of imaging features that included tumor size, location, depth (superficial or deep), types of margin, calcification, internal septa, cystic component, hemorrhage, fluid-fluid level, triple signal pattern, signal characteristics on T1- and T2-weighted images, and homogeneity (homogeneous or heterogeneous). Superficial tumor (dermal or subcutaneous tumor) was exclusively located above the superficial fascia without invasion of the fascia. Deep tumor was located either exclusively beneath the superficial fascia or superficial to the fascia with invasion of or through the fascia. Tumors arising from the knee, ankle, foot, forearm, and hand were included in the distal lesions. Tumors arising from the neck, trunk, femur, and inguinal regions were contained in the proximal lesions.

The signal characteristics were mainly described as isointense or hyperintense relative to the signal intensity of skeletal muscle. Triple signal pattern—characterized by the presence of high signal similar to that of fluid, intermediate signal intensity equal to or slightly hyperintense relative to fat, and low signal intensity closer to that of fibrous tissue—was also noted. Enhancement of the lesion signal intensity was assessed after contrast material injection and was categorized as either none, weak, or marked compared with those of the surrounding skeletal muscles. Homogeneity of enhancement was categorized as homogeneous or heterogeneous and also recorded.

Statistical Analysis

The demographics and imaging characteristics of patients were compared using the Wilcoxon rank sum test for continuous variables and the χ^2 or Fisher exact test probability tests for categorized variables. Univariate analysis was performed by comparing Kaplan-Meier survival curves and carrying out log-rank tests. The relative risk of each variable subjected to multivariate analysis was estimated using a Cox proportional hazards model. All analyses were conducted using SPSS software (version 11.0J; SPSS, Chicago, IL). Differences and correlations at a P value of <0.05 was considered to be statistically significant.

RESULTS

The median age at the time of presentation was 27 years and 9 patients (30%) were under 20 years of age. The tumors were located on the extremities in 22 (73%) pateints, trunk in 7 (23%), and neck in 1 (4%). The median tumor size was 7 cm and ranged from 2.2 to 15.0 cm. Twenty-five (83%) tumors were situated deeply, and 5 (17%) were superficial. The surgical procedures performed consisted of wide excision, amputation, or disarticulation with adequate surgical margins in 17 (57%) patients and marginal or intralesional excision with marginal or inadequate margins in 14 (43%). Additional treatment included chemotherapy in 22 (73%) patients, radiotherapy in 1 (3%), and both in 5 (17%). Metastases occurred in 11 (37%) of the 30 patients, and the locations were the lung in 6 (20%) patients, soft tissue in 2 (7%), bone in 2 (7%), brain in 2 (7%), and abdominal dissemination in 2 (7%), respectively. Nine (30%) patients developed local recurrences.

On both CT and MR images, 16 (53%) and 14 (47%) of 30 tumors had regular and irregular tumor contours, respectively. Twenty-two (73%) tumors were attached or located adjacent to muscular tendons. Calcifications that appeared as

round, punctate (Fig. 1) and dense (Fig. 2) were identified on unenhanced CT images in 3 (10%) low-grade and 5 (17%) high-grade tumors, respectively. The lesion usually appeared as a heterogeneous soft tissue mass and may have a multilocular appearance with various degrees of internal septations. On T2-weighted MR images, tumors predominately showed increased signal intensity relative to that of the skeletal muscle (Fig. 3), and the images showed heterogeneous appearance with internal septa of low intensity. Internal septa were found in 20 (67%) tumors on T2-weighted MR images. Cystic components (Fig. 4) were seen in 19 (63%) patients with high-grade tumor. Of these, 4 (13%) cases showed multilocular cystic lesions within the tumor. High intensity signals on T1-weighted MR images highly suggestive of hemorrhage (Fig. 3) were found in 14 (47%) patients with high-grade tumors. Of these tumors associated with hemorrhage, 5 (17%) tumors contained fluid-fluid levels on T2-weighted MR images. Triple signal pattern (Fig. 5) was seen in 13 (43%) patients with high-grade tumor. All tumors showed marked enhancement compared with those of the adjacent skeletal muscles on contrast-enhanced MR images. Contrast-enhanced MR images revealed homogeneous and heterogeneous enhancement (Fig. 4) in 5 (17%) and 25 (83%) tumors, respectively.

The results of the statistical analysis are summarized in Tables 1 to 3. Statistically significant imaging findings favoring a diagnosis of high-grade tumor included proximal distribution ($P < 0.01$), large tumor size (>10 cm; $P < 0.05$), the absence of calcification ($P < 0.05$), tumor possessing cyst ($P < 0.01$), the presence of hemorrhage ($P < 0.05$), and the presence of triple signal pattern ($P < 0.05$). Imaging features including cyst, hemorrhage, triple signal pattern, and fluid-fluid levels were found only in high-grade tumors. At the last follow-up, 9 of the 30 (30%) patients had died of their disease and 21 (70%) were alive with or without metastatic disease, with 5-year DFS rates of 48%. Both MFS and RFS rates were 58% and 65%, respectively. There was a significant difference in 5-year DFS rates between low- and high-grade tumors (100% vs. 26%, $P < 0.05$). Significant difference was also found in the MFS between low- and high-grade tumors (100% vs. 14%, $P < 0.05$) whereas not in the RFS (100% vs. 47%, $P = 0.07$). The univariate analysis revealed that proximal distribution ($P < 0.05$; Fig. 6), tumor size larger than 5 cm ($P < 0.01$, Fig. 7), the absence of calcification ($P < 0.01$; Fig. 8), the presence of hem-

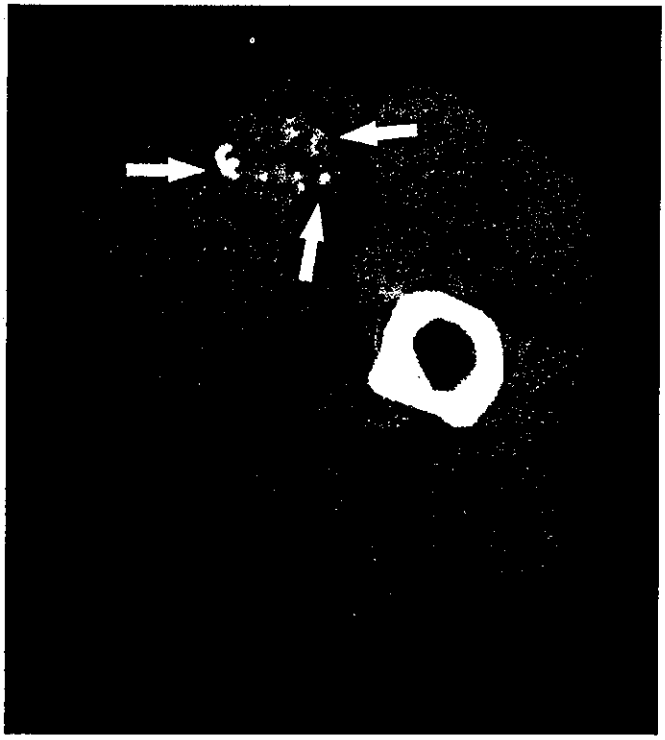

FIGURE 1. Unenhanced CT image obtained in a 14-year-old woman with synovial sarcoma (low-grade) of left groin. Image obtained at the level of inguinal region shows round or punctate calcifications (arrows) within the tumor.

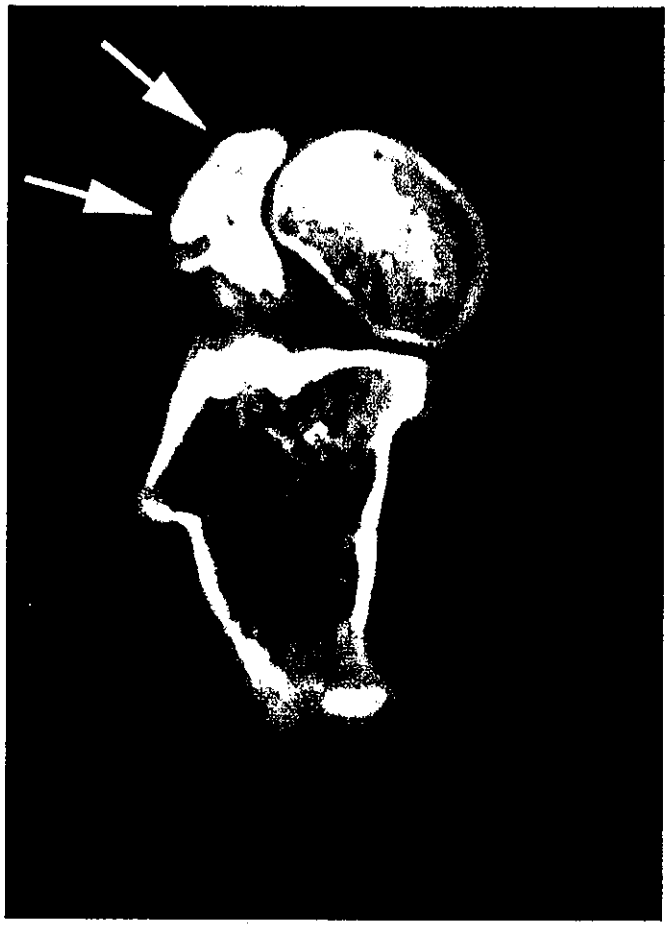

FIGURE 2. Unenhanced CT image obtained in a 14-year-old boy with synovial sarcoma (low-grade) of left foot. Image obtained at the level of talus head shows a dense calcification (arrows).

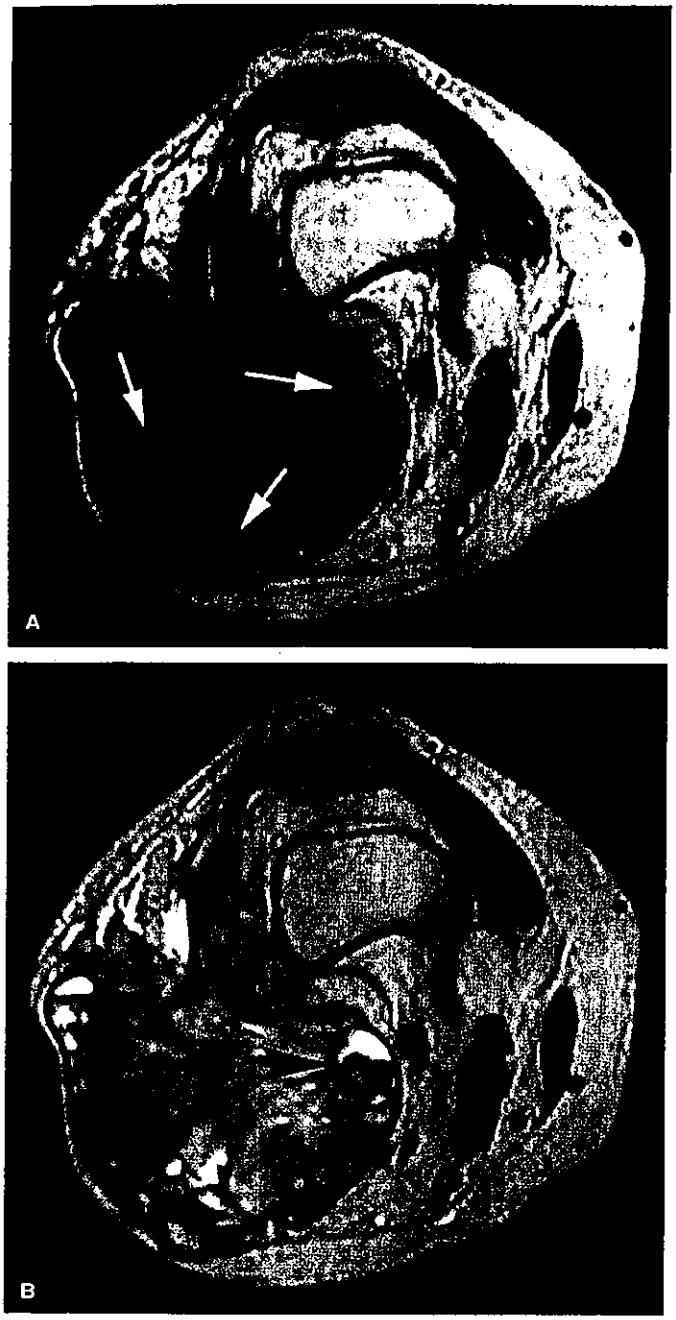

FIGURE 3. A 57-year-old woman with synovial sarcoma (high-grade) in left knee. A, Axial T1-weighted spin-echo (TR/TE: 720/50 milliseconds) MR image at the level of distal femur shows irregular soft tissue mass with multiple areas of high intensity signals (arrows). B, Axial T2-weighted fast spin-echo (3500/100) MR image shows fluid-fluid that suggests the presence of hemorrhage at the same location (arrowheads).

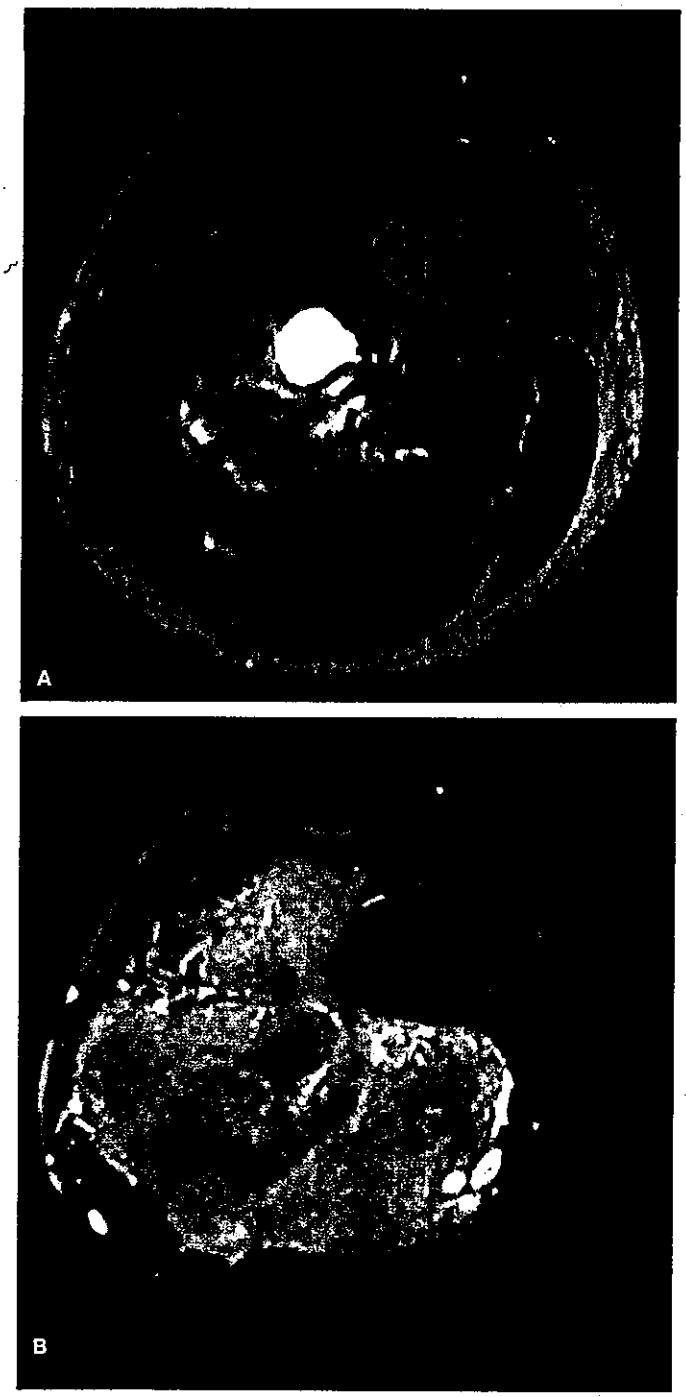

FIGURE 4. A 17-year-old man with synovial sarcoma (high-grade) in left thigh. A, Axial T2-weighted fast spin-echo (3500/100) MR image at the level of femur shows a large irregular mass of heterogeneous signal intensity. Also noted is central cystic degeneration (arrowhead). B, Fat-suppressed contrast-enhanced T1-weighted spin-echo (650/12) MR image demonstrates heterogeneous enhancement.

orrhage ($P < 0.05$; Fig. 9), and the presence of triple signal pattern ($P < 0.05$; Fig. 10) had a significant association with the DFS (Table 1). No significant impact on the DFS was found in patients' age, gender, operative margins, or with or without

FIGURE 5. A 19-year-old woman with synovial sarçoma (high-grade) in right buttock. A, Coronal T2-weighted fast spin-echo (3500/100) MR image demonstrates triple signal pattern that includes high signal similar to that of fluid (arrows), intermediate signal intensity equal to or slightly hyperintense relative to fat (arrowheads), and low signal intensity closer to that of fibrous tissue (asterisk).

additional chemotherapy and radiotherapy. Imaging features including large tumor size ($P < 0.05$), the presence of internal septa ($P < 0.05$), and the presence of fluid-fluid levels ($P < 0.05$) were significantly associated with the MFS (Table 2). No statistically significant association was found between the RFS and the clinical or imaging features. Multiple logistic regression model showed that tumor size larger than 10 cm had a significant impact on the DFS with relative risk of 18.8 (95% confidence interval, 1.8–194.0, $P < 0.05$).

DISCUSSION

In the current study we have documented the prognostic significance of CT and MR imaging features in patients with synovial sarcoma of the soft tissues. Univariate analysis revealed that proximal distribution, hemorrhage, triple signal pattern, and calcification were significantly associated with overall survival. Synovial sarcomas of the soft tissues have been described as malignant mesenchymal tumors of uncertain origin with 5- and 10-year survival rates of 24% to 64% and 11% to 34%, respectively.[1,6] From a practical viewpoint, it seems useful to detect these imaging findings on CT or MR images in synovial sarcoma of the soft tissues to predict their behavior.

The radiologic appearance of smaller lesions can be well circumscribed and homogeneous, but is more frequently calcified than other soft tissue sarcomas. Calcification, present in approximately 30% of adult cases, may distinguish this lesion from other soft tissue sarcomas.[6,7] Twenty-eight percent of our cases had calcification within the tumor on CT scans which closely mirrored other published findings. Additionally, calcification in the stroma has been reported as a prognostic factor.[6] In our series, absence of calcification was a significant imaging finding favoring a diagnosis of high-grade tumor and was also significantly associated with poor prognosis. Therefore, to detect calcifications of synovial sarcoma of the soft tissues may be considered important and should be interpreted with CT scans.

High signal intensity on T1- and T2-weighted images corresponded to areas of hemorrhage identified pathologically as described in previous studies.[8,9] In our results, hemorrhage was found only in 12 patients with high-grade tumors and was a significant adverse prognostic factor. Triple signal pattern, one of the heterogeneous patterns on T2-weighted MR images, was also a significant adverse prognostic factor. Triple signal is considered to be not specific, but suggestive of the diagnosis given the most prevalent age.[8] Therefore, to detect this finding on T2-weighted MR images is relevant when evaluating patients with synovial sarcoma of the soft tissues. Fluid-fluid levels may occur whenever substances of differing densities are contained within a cystic or compartmentalized structure. The levels are depicted when imaging is performed in a gravity-dependent plane. Malignant tumors are often multiloculated, representing trapped fluid compartmentalized by thin bands of viable tumor. The presence of fluid-fluid levels in soft tissue tumors cannot be considered diagnostic of any particular tumor, including synovial sarcoma, hemangioma, or malignant fibrous histiocytoma.[18] A sign of fluid-fluid level was seen in 4 of our cases on T2-weighted MR images, which would suggest that this finding might be noteworthy but not specific in synovial sarcoma of the soft tissues. Concerning fluid-fluid levels, the MR appearance of mixed signal is often termed "bowl of fruit" because the various signal intensity areas resemble a collection of fruits, but this finding is not specific to synovial sarcoma and is also seen in malignant fibrous histiocytoma.[10] These MR findings of our cases, which included a heterogeneous, multilocular configuration with varying degrees of internal septa with or without fluid-fluid levels, agreed with those in previous descriptions of synovial sarcoma.[8]

Synovial sarcomas do not seem to enhance as markedly as tumors of vascular origin and are heterogeneous owing to the presence of degeneration including cyst, hemorrhage, or calcified regions of the tumor.[8–18] Tumors tend to have intermediate signal intensity on T1-weighted MR images. The T2-weighted signal intensity depends on the cellularity of the neoplasm; highly cellular types usually show intermediate signal intensity on T2-weighted images, and the stromal or less cellular variety have high T2-weighted signal intensity.[8–13] Fujimoto et al[11] reported a single case of synovial sarcoma of the chest wall in which the areas of low signal intensity on T1- and T2-weighted images corresponded to viable fibrous tissue of the tumor on pathologic correlation. The authors also de-

TABLE 1. Prognostic Factors for Disease-Free Survival (DFS) in Patients with Synovial Sarcoma of the Soft Tissues

Variable	5-Year DFS Rate (%)	n (%)	*P* Value
Age			0.39
<20 years	58	8 (26.7)	
≧20years	54	22 (73.3)	
Gender			0.59
Male	58	12 (40.0)	
Female	44	18 (60.0)	
Site			<0.05
Distal	89	13 (43.3)	
Proximal	23	17 (56.7)	
Size			<0.01
≦5 cm	86	12 (40.0)	
5–10 cm	0	10 (33.3)	
>10 cm	18	8 (26.7)	
Surgical margin			0.48
Adequate	47	16 (53.3)	
Inadequate	54	14 (46.7)	
Depth			0.61
Superficial	67	5 (16.7)	
Deep	43	25 (83.3)	
Stage			<0.01
IA	100	6 (20.0)	
IB	100	2 (6.7)	
IIB	100	8 (26.7)	
III	100	3 (10.0)	
IV	0	11 (36.7)	
Adjuvant therapy			0.14
None	88	8 (26.7)	
CTX and/or RTX	27	22 (73.3)	
Internal septa			0.09
Positive	80	10 (33.3)	
Negative	27	20 (66.7)	
Cyst			0.14
Positive	27	19 (63.3)	
Negative	78	11 (36.7)	
Calcification			<0.01
Positive	100	22 (73.3)	
Negative	0	8 (26.7)	
Hemorrhage			<0.05
Positive	0	16 (53.3)	
Negative	75	14 (46.7)	
Fluid-fluid levels			0.20
Positive	38	5 (16.7)	
Negative	50	25 (83.3)	
Triple signal pattern			<0.05
Positive	0	13 (43.3)	
Negative	76	17 (56.7)	
Enhancement			0.29
Homogeneous	75	5 (16.7)	
Heterogeneous	40	25 (83.3)	

Note: CTX, chemotherapy; RTX, radiotherapy.

TABLE 2. Prognostic Factors for Metastasis-Free Survival (MFS) in Patients with Synovial Sarcoma of the Soft Tissues

Variable	5-Year MFS Rate (%)	n (%)	*P* Value
Age			0.80
<20 years	60	8 (26.7)	
≧20 years	56	22 (73.3)	
Gender			0.93
Male	47	12 (40.0)	
Female	60	18 (60.0)	
Site			0.11
Distal	81	13 (43.3)	
Proximal	43	17 (56.7)	
Size			<0.05
≦5 cm	89	12 (40.0)	
5–10 cm	42	10 (33.3)	
>10 cm	31	8 (26.7)	
Surgical margin			0.25
Adequate	68	16 (53.3)	
Inadequate	46	14 (46.7)	
Depth			0.42
Superficial	67	5 (16.7)	
Deep	55	25 (83.3)	
Stage			<0.0001
IA	100	6 (20.0)	
IB	100	2 (6.7)	
IIB	100	8 (26.7)	
III	100	3 (10.0)	
IV	0	11 (36.7)	
Adjuvant therapy			0.30
None	75	8 (26.7)	
CTX and/or RTX	48	22 (73.3)	
Internal septa			<0.05
Positive	86	10 (33.3)	
Negative	45	20 (66.7)	
Cyst			0.24
Positive	68	19 (63.3)	
Negative	52	11 (36.7)	
Calcification			0.34
Positive	70	22 (73.3)	
Negative	52	8 (26.7)	
Hemorrhage			0.07
Positive	70	16 (53.3)	
Negative	44	14 (46.7)	
Fluid-fluid levels			<0.05
Positive	40	5 (16.7)	
Negative	62	25 (83.3)	
Triple signal pattern			0.11
Positive	41	13 (43.3)	
Negative	71	17 (56.7)	
Enhancement			0.64
Homogeneous	60	5 (16.7)	
Heterogeneous	58	25 (83.3)	

Note: CTX, chemotherapy; RTX, radiotherapy.